Int J Fract (2019) 216:135–148
https://doi.org/10.1007/s10704-019-00347-z

ORIGINAL PAPER

Intergranular fracture prediction and microstructure design

Shmuel Osovski · Alan Needleman · Ankit Srivastava

Received: 6 October 2018 / Accepted: 24 January 2019 / Published online: 4 March 2019

Abstract A model based on discrete unit events coupled with a graph search algorithm is developed to predict intergranular fracture. The model is based on two hypotheses: (i) the key unit event associated with intergranular crack propagation is the interaction of a grain boundary crack with a grain boundary segment located at an angle with the initial crack plane; and (ii) for a given crack path, the overall crack growth resistance can be calculated using the crack growth resistance of a collection of unit events. Next, using a directed graph containing the connectivity of grain boundary junctions and the distances between them, and crack deflection versus crack growth resistance data, a directed graph in the J-resistance space is created. This graph contains information on the crack growth resistance for all possible crack paths in a given grain microstructure. Various crack growth resistance curves are then calculated including those corresponding to: (i) a local resistance minimum; (ii) a global minimum; and (iii) for verification, a path specified by microstructure-based finite element calculations. The results show that the proposed method based on discrete unit events and graph search can predict the crack path and the crack growth resistance for cracks that propagate from one grain boundary junction to another. The proposed computationally inexpensive model can be used to design material microstructures with improved intergranular fracture resistance, and/or to assess the overall crack growth resistance of materials with a known distribution of grain morphology.

Keywords Grain boundaries · Crack path · Fracture toughness · Graph search · Microstructure design

S. Osovski
Faculty of Mechanical Engineering, Technion - Israel Institute of Technology, Haifa, Israel

A. Needleman · A. Srivastava (✉)
Department of Materials Science and Engineering, Texas A&M University, College Station, TX, USA
e-mail: ankit.sri@tamu.edu

1 Introduction

The increasingly demanding requirements for lower fuel consumption and for lower CO_2 emissions drives design toward lightweight structures in weight-critical applications such as for aircraft and for long-haul trucks. High levels of reliability are also required in these applications. Hence, there is an increasing desire to use structural materials with high specific strength (strength to weight ratio). Examples of materials with high specific strength include Al–Li alloys and high strength metastable β titanium alloys. Unfortunately, these materials are prone to grain boundary ductile fracture that limits their use in fracture-critical components or structures. Here, we propose a novel methodology for designing material microstructures with improved crack growth resistance for materials that are prone to grain boundary ductile fracture. The proposed methodology can also be used to assess the overall crack growth

resistance of materials with a known distribution of key microstructural features.

The past few decades have seen rapid advances in inverse design methodologies that facilitate material design to achieve a targeted performance metric (Olson 1997; McDowell 2007; McDowell and Olson 2009; Fullwood et al. 2010; Liu et al. 2015). However, relatively few studies have been aimed at designing high toughness ductile materials (Hao et al. 2003, 2004; Kulkarni et al. 2004). In Hao et al. (2003, 2004) the focus was on fracture initiation in steels and the effects of microstructural heterogeneities, such as void nucleating particle distributions and grain morphology. Also, in these works the material microstructure entered the design space in a homogenized way, i.e. the material microstructure was smeared out and/or defined in terms of correlation functions.

In Srivastava et al. (2017) it was shown that the ductile crack growth resistance of a material is strongly affected by the crack path and to the extent it is possible to engineer the crack path, the crack growth resistance can be increased by designing the material microstructure. Thus, material design involving crack path engineering to increase the crack growth resistance involves optimizing the topological features of the materials microstructure. Various topology optimization schemes have been applied to continuum and discrete structures with the aim of designing optimal structural layouts for a variety of design objectives, e.g. Bendsøe and Kikuchi (1988), Kirsch (1990), Cheng and Jiang (1992), Chapman et al. (1994), Bendsøe and Sigmund (2004), van Dijk et al. (2013), James and Waisman (2014), Xia and Breitkopf (2015).

Topology optimization techniques have been used to design composite microstructures with desirable properties, e.g. Sigmund and Torquato (1997), Larsen et al. (1997), Sigmund et al. (1998), Hyun and Torquato (2001), Torquato and Hyun (2001), Torquato (2005). Topological optimization of composite materials has usually been focused on optimizing properties that can be found by homogenizing the local fields in the microstructure. This, to an extent, allows using approximate (but efficient) finite element models of the composite microstructure coupled with an iterative optimization scheme within a single computational framework. However, full field microstructure-based finite element calculations of crack growth in a specified microstructure as in Osovski et al. (2015a), Srivastava et al. (2017) are very computationally expensive so that direct coupling of such calculations with an iterative optimization scheme is not practical.

The microstructure-based finite element modeling in Osovski et al. (2015a) focused on understanding the effects of material properties and grain microstructural features on the crack growth resistance of metastable β titanium alloys. The microstructure of metastable β titanium alloys consists of hard grains of β phase embedded within α phase laths, and with a soft α phase layer along the grain boundaries (Lütjering and Williams 2007). This microstructure leads to grain boundary ductile fracture at room temperature (Williams et al. 1978; Lütjering and Williams 2007; Mantri et al. 2015). The results of the microstructure-based finite element modeling (Osovski et al. 2015a) show that changes in grain morphology affect both the crack growth initiation toughness and the tearing modulus (slope of the crack growth resistance curve). However, all the calculated crack growth resistance curves exhibited one common feature, namely a piecewise linear relation between crack growth resistance and crack extension that is occasionally perturbed by jumps in crack growth resistance. The slope of the crack growth resistance curve was correlated with the morphology of the grain boundary network, whereas the jumps in crack growth resistance were found to be due to the interaction of the propagating crack with grain boundary junctions.

The analyses in Osovski et al. (2015a) suggest that the crack growth resistance of a crack propagating through a grain boundary network can be described by discrete unit events. Based on these observations we formulate two hypothesis: (i) the key unit event associated with intergranular crack propagation is the interaction of a grain boundary crack with a grain boundary segment located at an angle with the initial crack plane; and (ii) for a given crack path, the crack growth resistance curve can be calculated using the crack growth resistance of a collection of unit events given the position, orientation and length of each grain boundary segment along the crack path is known.

Here, the hypotheses formulated based on the analyses of Osovski et al. (2015a) are used to develop a simple model based on discrete unit events coupled with a graph search algorithm to predict intergranular fracture in various grain microstructures. The relationship between the angle of crack deflection (due to the interaction of a grain boundary crack with a grain boundary junction) and the associated crack growth resistance

for a unit length of crack is carried out via a series of unit event microstructure-based finite element calculations. Next, the network of grain boundaries is constructed via a centroidal Voronoi tessellation scheme and is mapped onto a graph, were each grain boundary junction is a node on the graph. The graph is constructed in Euclidean space and all trajectories are extracted using a breadth-first search algorithm (Lee 1961). To calculate the crack growth resistance curve of a given crack path along the grain boundary network, a similar graph is built in the J-resistance space using the crack deflection versus crack growth resistance data. Once constructed, the graph contains information as to all possible crack growth paths in a given microstructure and their corresponding crack growth resistance curves. Finally, the path of least resistance is found by utilizing Dijkstra's algorithm (Dijkstra 1959). Dijkstra's algorithm is a graph search algorithm that produces the minimal distance between a given node and any other node on the graph. The distances in this case are the increments in crack growth resistance resulting from a crack traveling between two nodes.

Calculations are carried out for grain microstructures representative of metastable β titanium alloys. The predictions are found to be in close agreement with the predictions of the full field microstructure-based finite element crack growth calculations. The comparison of the predictions of our simple model and the finite element calculations also shows that the final crack path in a specified microstructure is not necessarily the path of least resistance. Because of its computational efficiency, the model proposed here has the potential for being employed in an iterative optimization scheme to design material microstructures with improved intergranular fracture resistance, and/or to assess the overall crack growth resistance of materials with a known distribution of grain boundaries.

2 Microstructure-based material model and numerical implementation

The microstructure-based numerical modeling is carried out to quantify the effect of grain morphology on crack growth resistance, as well as to calibrate and validate the simplified model formulated based on the graph search method presented in Sect. 3. The material model and the numerical implementation are the same as in Needleman et al. (2012), Srivastava et al. (2014, 2017), Osovski et al. (2015a, b). Here, for completeness, we briefly describe the formulation. More complete descriptions are given in the references cited.

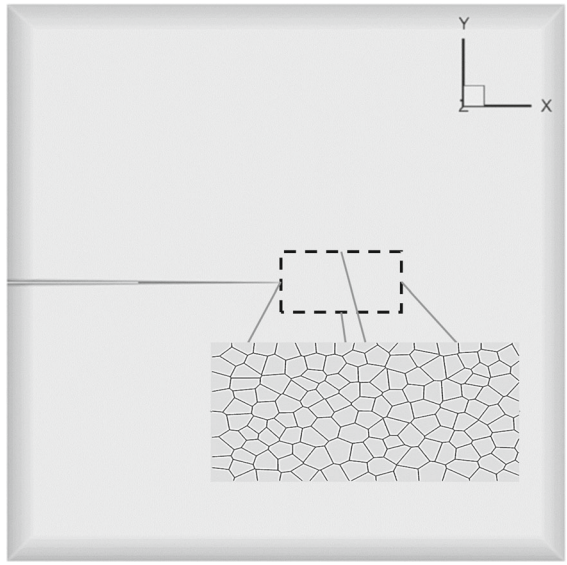

Fig. 1 Sketch of the initially cracked slice of material analyzed, showing the grain microstructure in the region in front of the initial crack tip

As in Needleman et al. (2012), Srivastava et al. (2014, 2017), Osovski et al. (2015a, b), we analyze a mode I small scale yielding boundary value problem for a slice of material with an initial crack, Fig. 1. The region analyzed has dimensions $h_x \times h_y \times h_z$ with boundary conditions on $z_0 = 0, h_z$ giving overall plane strain. The initial and boundary displacement and velocity fields corresponding to the isotropic elastic mode I plane strain singular field are applied. For small scale yielding the value of J is related to the imposed stress intensity factor K_I by Rice (1968)

$$J = K_I^2 \frac{\left(1 - \nu^2\right)}{E} \tag{1}$$

where ν is Poisson's ratio and E is Young's modulus. A monotonically increasing remote stress intensity factor, $K_I(t)$ is prescribed with $\dot{K}_I = 1.2 \times 10^7\ \mathrm{MPa}\sqrt{\mathrm{m}}\mathrm{s}^{-1}$.

A finite deformation, finite element formulation based on the dynamic principle of virtual work is used. The finite element formulation is three dimensional, using twenty-node brick elements and the internal force contributions are integrated using eight point Gaussian integration. The explicit Newmark β-method, with

$\beta = 0$, Belytschko et al. (1976) is used for time integration. Here, the microstructure is taken to be constant through the slice thickness with only one element through the thickness h_z so that the deformation field is essentially two dimensional plane strain. A uniform in-plane ($x_0 - y_0$ plane) mesh is used in a region in front of the initial crack tip in which the material microstructure is modeled as shown schematically in Fig. 1. The material modeled consists of a soft α phase layer surrounding hard grains. The hard grains, referred to as β grains, mainly consist of β Ti but have embedded α phase laths. Here, the grains are modeled as homogeneous and isotropic.

The grain microstructure in the region in front of the initial crack tip is generated using a centroidal Voronoi tessellation scheme as described in Osovski et al. (2015a). First, Ng random points are assigned in the region where the microstructure is modeled, Fig. 1. Each random point acts as a generator for a Voronoi cell (grain). For each cell, the distance between its generator and its center of mass is calculated and a new generator is created to minimize that distance. The asymptotic limit of this iterative scheme in 2D results in a perfectly equiaxed microstructure. To generate the grain boundaries each Voronoi cell is shrunk so that a distance equal to half the desired α layer width (grain boundary) is generated between the original and new cell faces. For all the calculations reported here the width of grain boundary α layer varies from 6 to 10 μm and the average grain size is $\approx 330\,\mu$m. The obtained list of polyhedrons is then projected onto the fine meshed region in front of the initial crack tip and each Gauss integration point in the finite element mesh is assigned the material/constitutive properties associated with the phase in which it lies. This procedure gives a microstructure with Ng grains.

The material model is a modified Gurson elastic-viscoplastic constitutive relation for a progressively cavitating solid as used in Osovski et al. (2015a). The flow potential given by Gurson (1975)

$$\Phi = \frac{\sigma_e^2}{\bar{\sigma}^2} + 2q_1 f^* \cosh\left(\frac{3q_2\sigma_h}{2\bar{\sigma}}\right) - 1 - \left(q_1 f^*\right)^2 = 0 \tag{2}$$

where $q_1 = 1.25$, $q_2 = 1.0$ are parameters introduced in Tvergaard (1981, 1982a), f is the void volume fraction, $\bar{\sigma}$ is the matrix flow strength and

$$\sigma_e{}^2 = \frac{3}{2}\boldsymbol{\sigma}' : \boldsymbol{\sigma}' \,,\ \sigma_h = \frac{1}{3}\boldsymbol{\sigma} : \mathbf{I} \,,\ \boldsymbol{\sigma}' = \boldsymbol{\sigma} - \sigma_h \mathbf{I} \tag{3}$$

with f^* given by Eq. (4) as introduced in Tvergaard and Needleman (1984)

$$f^* = \begin{cases} f, & f < f_c \\ f_c + (1/q_1 - f_c)(f - f_c)/(f_f - f_c), & f \geq f_c \end{cases} \tag{4}$$

where the values $f_c = 0.12$ and $f_f = 0.25$ are used.

The rate of deformation tensor is written as the sum of an elastic part, $\mathbf{d}^e = \mathbf{L}^{-1} : \hat{\boldsymbol{\sigma}}$, a viscoplastic part, $\mathbf{d}^p$, and a thermal straining contribution, $\mathbf{d}^\Theta = \alpha\dot{\Theta}\mathbf{I}$

$$\mathbf{d} = \mathbf{L}^{-1} : \hat{\boldsymbol{\sigma}} + \alpha\dot{\Theta}\mathbf{I} + \mathbf{d}^p \tag{5}$$

Here, $\hat{\boldsymbol{\sigma}}$ is the Jaumann rate of Cauchy stress, Θ is the temperature, $\alpha = 1 \times 10^{-5}$/K is the thermal expansion coefficient and $\mathbf{L}$ is the tensor of isotropic elastic moduli.

The plastic part of the strain rate, $\mathbf{d}^p$, as given in Pan et al. (1983) is

$$\mathbf{d}^p = \left[\frac{(1-f)\bar{\sigma}\dot{\bar{\epsilon}}}{\boldsymbol{\sigma} : \frac{\partial\Phi}{\partial\boldsymbol{\sigma}}}\right]\frac{\partial\Phi}{\partial\boldsymbol{\sigma}} \tag{6}$$

The matrix plastic strain rate, $\dot{\bar{\epsilon}}$, is given by

$$\dot{\bar{\epsilon}} = \dot{\epsilon}_0\left[\frac{\bar{\sigma}}{g(\bar{\epsilon},\Theta)}\right]^{1/m} \,,\ g(\bar{\epsilon},\Theta) = \sigma_0 G(\Theta)\left[1 + \bar{\epsilon}/\epsilon_0\right]^N \tag{7}$$

with $\bar{\epsilon} = \int \dot{\bar{\epsilon}} dt$ and $\epsilon_0 = \sigma_0/E$. The elastic constants $E = 116$ GPa and $\nu = 0.3$ were taken to be the same for both phases as well as the hardening and rate sensitivity parameters given by $N = 0.1$, $m = 0.01$ and $\dot{\epsilon}_0 = 10^3 \mathrm{s}^{-1}$. The flow strength of the β phase grains, σ_0^β is taken to be 1200 MPa and for the α phase layer $\sigma_0^\alpha = 800$ MPa.

Adiabatic conditions are assumed so that

$$\rho c_p \frac{\partial\Theta}{\partial t} = \chi\boldsymbol{\tau} : \mathbf{d}^p \tag{8}$$

with $\rho = 4500$ kg/m^3 $= 4.5 \times 10^{-3}$ MPa/(m/s)^2, $c_p = 520$ J/(kg °K), $\chi = 0.9$, and the temperature-dependence of the flow strength is given by

$$G(\Theta) = 1 + b_G \exp(-c[\Theta_0 - 273]) \times \left[\exp(-c[\Theta - \Theta_0]) - 1\right] \quad (9)$$

with $b_G = 0.1406$ and $c = 0.00793$/K and $\Theta_0 = 293$ K.

The initial void volume fraction is taken to be zero and the evolution of the void volume fraction is governed by

$$\dot{f} = (1 - f)\mathbf{d}^p : \mathbf{I} + \dot{f}_{nucl} \quad (10)$$

where the first term on the right hand side of Eq. (10) accounts for void growth and the second term for void nucleation.

Since fracture in β metastable Ti alloys mainly occurs along grain boundaries (in the α phase layer) the α phase layer is taken to nucleate voids at early stages of the deformation process following the stress controlled nucleation criterion

$$\dot{f}_{nucl}^{\text{stress}} = A\left(\dot{\bar{\sigma}} + \dot{\sigma}_h\right), \quad A = \frac{f_N^{\text{stress}}}{s_N^{\text{stress}}\sqrt{2\pi}} \exp\left[-\frac{1}{2}\left(\frac{\bar{\sigma}+\sigma_h-\sigma_N}{s_N^{\text{stress}}}\right)^2\right] \quad (11)$$

if $(\bar{\sigma} + \sigma_h)$ is at its maximum over the deformation history. Otherwise $A = 0$. Here, $f_N^{\text{stress}} = 0.06$, $\sigma_N = 1.5\sigma_0$ and $s_N = 0.3$.

Plastic strain controlled void nucleation is taken to occur both in the β grains and in the grain boundary α phase layer via

$$\dot{f}_{nucl}^{\text{strain}} = D\dot{\bar{\epsilon}}, \quad D = \frac{f_N^{\text{strain}}}{s_N^{\text{strain}}\sqrt{2\pi}} \exp\left[-\frac{1}{2}\left(\frac{\bar{\epsilon}-\epsilon_N}{s_N^{\text{strain}}}\right)^2\right] \quad (12)$$

with $f_N^{\text{strain}} = 0.04$, $\epsilon_N = 0.2$ and $s_N = 0.2$ for both phases.

The constitutive updating is based on the rate tangent modulus method in Peirce et al. (1984) and failure is implemented using the element vanish technique of Tvergaard (1982b). When $f^* = 0.9 f_f$, the value of f^* is kept fixed so that the material deforms with a very small flow strength. The entire element is taken to have failed (zero stress carrying capacity) once three Gauss integration points in the element have met this condition. The extent of crack growth, Δa, beyond the initial crack is defined as the maximum projected length on the x-axis of the void volume fraction contour $f = 0.1$ as in Srivastava et al. (2014, 2017), Osovski et al. (2015a, b).

3 Modeling intergranular cracking as a graph search

The motivation for the graph search model comes from the numerical simulations in Osovski et al. (2015a). Those simulations of ductile crack growth in metastable β titanium alloys gave results for the effect of changes in grain morphology on: (i) the crack growth initiation toughness, J_{Ic}; and (ii) the tearing modulus (the slope of the $J - R$ curve), $T_R = \left(E/\sigma_0^2\right) dJ/d(\Delta a)$, (Paris et al. 1979). All the crack growth resistance curves in Osovski et al. (2015a) exhibited a piecewise linear relation between J and Δa that are occasionally perturbed by jumps in the value of J. The variation in the tearing modulus T_R was correlated with the morphology of the grain boundaries that acted as a network through which the crack propagates. The jumps in the value of J were found to be due to the interaction of the propagating crack with the grain boundary junctions. When a propagating crack reached a grain boundary junction, it remained there until sufficient weakening occurred on one of the grain boundary facets comprising the (triple) junction. This suggested that the crack growth resistance for a crack propagating through a grain boundary network could be described as a collection discrete unit events.

Based on the results in Osovski et al. (2015a), our first hypothesis is that the unit event to be modeled is the interaction of a grain boundary crack with grain boundary α layers located symmetrically at an angle ψ about the crack plane (the inset of Fig. 2a shows this configuration for the specific case $\psi = 45°$). To obtain a relationship between the angle of crack growth, ψ, and the associated change in the value of J required for a unit length of propagation, we carried out a series of finite element calculations using the formulation presented in Sect. 2. Calculations were carried out for the configuration shown in the inset of Fig. 2a with values of ψ ranging from 0° to 85°. The variation of tearing modulus, T_R, and increment in crack growth resistance, ΔJ, with the crack deflection angle, ψ, are shown in Fig. 2a. The results shown in Fig. 2a provide the unit event data for our proposed model to predict intergranular cracking.

Our second hypothesis is that knowing the position, orientation and length of each grain boundary α segment for a given crack path, the crack growth resistance curve can be calculated using the unit event data in Fig. 2a. Thus, for a given grain morphology, the crack growth resistance curve, J versus Δa, can be calculated for any crack path emanating from the initial crack tip. To this end, the network of grain boundary α is constructed following the previously described Voronoi tessellation scheme. The obtained network of grain boundary α is then mapped onto a graph, were each grain boundary junction is represented by a node on the graph. Following this, the connectivity map is constructed such that flow on the graph is restricted to the direction of crack propagation (i.e. an increasing value of the crack length projected on the x-axis). The graph is constructed in Euclidean space so that all trajectories which traverse the graph up to a given distance can be extracted using a breadth-first search algorithm (Lee 1961). Next, to calculate the crack growth resistance curve for a given crack path along the grain boundary network, the energetic cost of crack propagating between the two nodes on the graph has to be known, i.e. a similar graph has to be built in J-resistance space. Using the unit event data in Fig. 2a in conjunction with the directed graph containing the connectivity of grain boundary junctions and the distances between them, a directed graph in the J-resistance space is created. The distances between the nodes in the Euclidean space and the propagation angle between them are input into the unit event model and the edge value of the new graph (i.e. the change in the value of J required to transverse the given edge) is obtained. A schematic representation of the directed graph in J-resistance space is shown in Fig. 2b.

The directed graph in the J-resistance space, Fig. 2b, contains information of the crack growth resistance curve for all possible crack paths in the microstructure. However, one needs to know the exact crack path to estimate the resultant crack growth resistance. The crack path for a specified amount of crack extension in the crack propagation direction can be estimated by finding the path with the least crack growth resistance, i.e. the path of global minimum resistance. The crack path for a specified amount of crack extension in the crack propagation direction can also be estimated by propagating the crack by a few grain boundary facets at a time based on some local minimum crack growth resistance criterion. The path of least resistance for the entire amount of the specified crack extension or for the cracks propagating a few grain boundary facets at a time can be estimated using Dijkstra's algorithm (Dijkstra 1959). Dijkstra's algorithm is a graph search algorithm that produces the minimal distance between two nodes. The distances in this case are the increments in J for a crack traversing between two nodes.

In Osovski et al. (2015a) it was shown that, for given material properties and a given grain microstructure, the value of J strongly depends on the offset between the initial crack tip and the nearest grain boundary that is not orthogonal to the initial crack. Thus, the value of J at the initiation of crack growth depends on a single event and can be highly variable. In Fig. 3a and subsequently, we focus on the effect of microstructure on crack growth following crack initiation so that the values of J plotted have the value of J at the initiation of crack growth subtracted. The values of J associated with crack growth following initiation depend on a collection of events associated with the entire grain microstructure and not just a single event. Figure 3a compares the crack growth resistance curves, J versus Δa, for crack paths estimated using four crack path selection criteria: (i) the global minimum resistance crack path for a specified amount of crack extension, $\Delta a = 11$ mm, (ii) a local minimum resistance crack path obtained by propagating the crack one grain boundary facet at a time and choosing the propagation path following the smallest value of T_R at the adjacent edges, (iii) a local minimum resistance crack path obtained by propagating one grain boundary facet at a time and choosing the propagation path by finding the nearest connected neighbor with smallest change in J, and (iv) a local minimum resistance crack path obtained by propagating two grain boundary facets at a time and choosing the propagation path based on the shortest path in terms of the change in J. The criteria (ii) can be thought of as the "most local" crack path selection criteria. The crack paths estimated using the four crack path selection criteria are shown in Fig. 3b. The $J - \Delta a$ curves obtained using all the four criteria in Fig. 3a are nearly identical for $\Delta a \approx 4.5$ mm but for $\Delta a > 4.5$ mm the global minimum criteria under predicts the crack growth resistance. One possibility is because the choice of the incremental crack path at a specific junction is not biased from the knowledge of what is to come next. Another possibility is that the unit event model does not account for the effects of events,

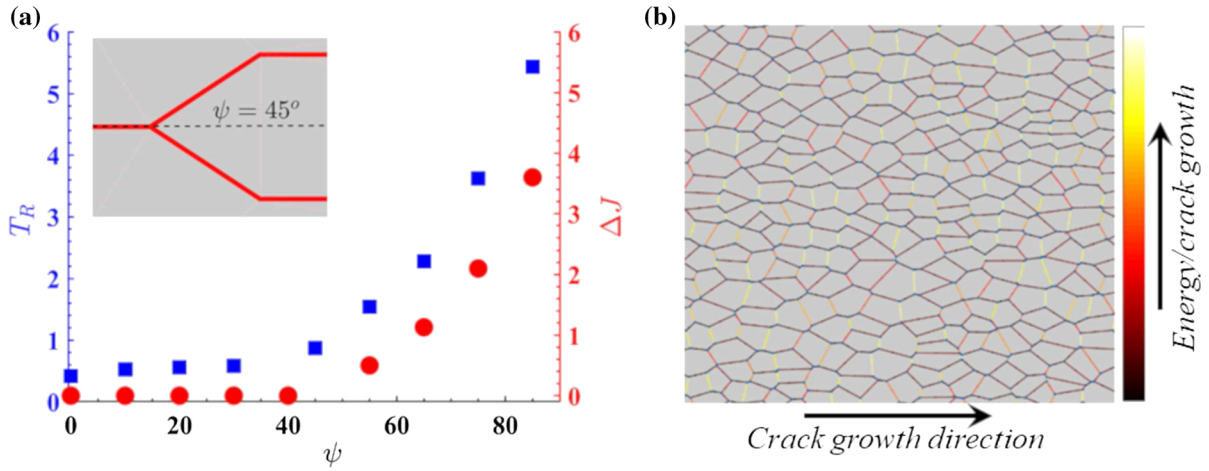

Fig. 2 **a** The tearing modulus, T_R, of a crack propagating along a grain boundary oriented at an angle ψ with respect to the plane of the propagating crack (closed squares) and the increment in crack growth initiation resistance, ΔJ, resulting from a crack reaching a triple junction as a function of ψ (closed circles). The inset in (**a**) shows a symmetric triple junction placed directly in front of the initial crack with an opening angle $\psi = 45°$. **b** A schematic representation of the graph describing the change in J required for the crack to propagate through the grain boundary network. The edges of the graph representing grain boundary α network are colored by the value of the required ΔJ to propagate through the grain boundary facet

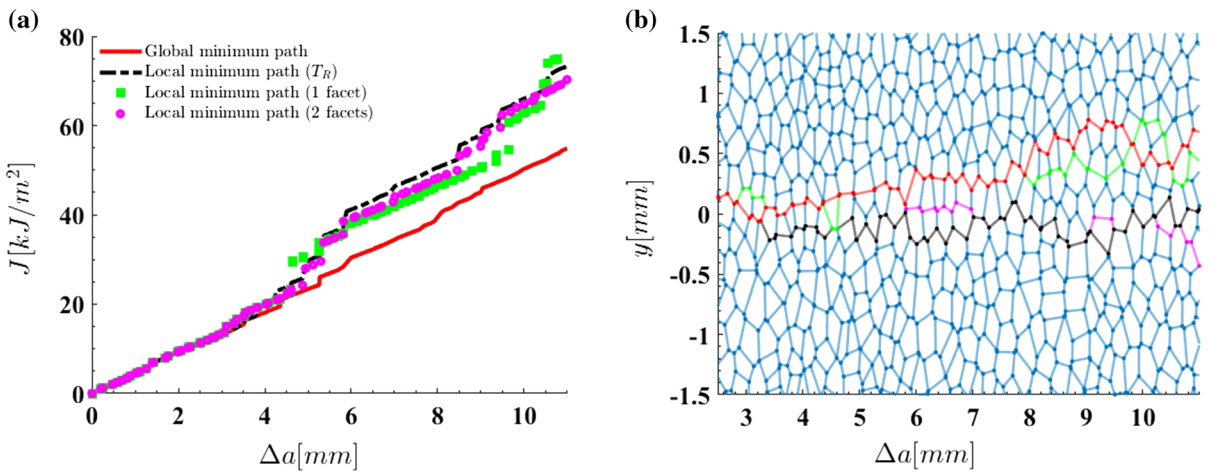

Fig. 3 The **a** crack growth resistance curves and corresponding **b** crack paths predicted using three local minimum crack growth resistance criteria and the global minimum crack growth resistance criterion

such as micro-cracking away from the main crack, that can occur ahead of the main crack tip.

4 Model prediction and validation

Two sets of crack growth resistance curves, J versus Δa, for two realizations of the same material microstructure are compared in Fig. 4. One set is obtained from full microstructure-based finite element calculations while the others were obtained using the unit event model and graph search. The two realizations of the grain microstructure are identical in terms of material properties and microstructural length scales (average grain boundary thickness and grain size), and only differ in the initial array of random generators for the Voronoi tessellation process. In Fig. 4a, b, J versus Δa curves are predicted using the proposed unit event model for three crack paths: (i) the crack path obtained from the full field microstructure-based finite element calculations (model prediction), (ii) the crack

path of minimum crack growth resistance for a specified crack extension, $\Delta a = 8$ mm (global minimum), and (iii) the crack path dictated by the local minimum crack growth resistance at each grain boundary junction (local minimum). The local minimum crack growth resistance crack path is determined by propagating the crack at each junction along the grain boundary giving the smallest change in the value of J for a given Δa until the crack has reached the specified $\Delta a = 8$ mm.

As noted in Sect. 3, the value of J at initiation i.e. the value at $\Delta a = 0$, depends strongly on the offset between the initial crack tip and the nearest grain boundary facet and is highly variable. Because our focus is on the effect of microstructure on the crack path, and, in turn, on the effect of crack path on crack growth resistance, the values of J plotted in Fig. 4a, b have the value of J at $\Delta a = 0$ in the unit event model and graph search predictions scaled to match the finite element results. The crack paths obtained from the microstructure-based finite element calculations and predicted using the proposed model based on global minimum and local minimum crack growth resistance criteria for the two realizations of the specified grain microstructure are shown in Fig. 5a, b, respectively.

As shown in Fig. 4a for realization 1, the J versus Δa curve predicted using the proposed model for the three crack paths and microstructure-based finite element calculations are nearly identical for $\Delta a < 4$ mm. The model predictions for all three crack paths differ from the results of the microstructure-based finite element calculations for $\Delta a > 4$ mm. This is because for realization 1, the finite element calculation exhibits crack branching, see Fig. 5a. Branching acts as additional toughening mechanism that is not account for in our model. On the other hand, the microstructure-based finite element calculation for realization 2 does not exhibit crack branching, Fig. 5b. In this case, the J versus Δa curve predicted using (i) the same crack path as in the microstructure-based finite element calculations (model prediction) and (ii) the crack path dictated by the local minimum crack growth resistance at each grain boundary junction (local minimum) are essentially identical to the J versus Δa curve obtained from the microstructure-based finite element calculations, Fig. 4b. Furthermore, for realization 2, the proposed model based on the global minimum criteria underpredicts the J versus Δa curve. This is because there is no a priori reason for a crack propagating in a given microstructure to choose the path of least global resistance.

5 An implication for microstructure design

The results presented in Sect. 4 clearly show that the computationally efficient unit event based model can predict the crack growth resistance of material microstructures that are prone to intergranular fracture. Possible routes to designing microstructures that increase the crack growth resistance are to increase the extent of crack deflection from the crack propagation direction and/or to promote crack meandering. Both of these increase the amount of new free surface created for a given amount of crack growth Δa. To quantify the scaling between the crack growth resistance and the extent of crack deflection from the crack propagation direction, we generated three realizations of a specified initial microstructure. For each realization the starting point of crack growth is chosen to be the node closest to the symmetry plane $y = 0$. All of the reachable nodes at $x = \Delta a$ and $| y | = \Delta y$ are chosen as targets and the crack path as well as the crack growth resistance are calculated using the global minimum resistance criterion. Figure 6a shows the variation in the value of J with the overall deviation from the symmetry plane, Δy, i.e. the height of the target node with respect to $y = 0$, at a specified Δa for the three realizations of the specified microstructure. A few representative crack paths corresponding to the crack growth resistance for realization 1 of the microstructure are shown in Fig. 6b. As seen in Fig. 6a, the J versus Δy curves for all three realizations follow the same master curve with $J = J_0 + k_1 \Delta y^{k_2}$, where $J_0 = 62.2$ is the overall crack growth resistance for the crack path with negligible crack deflection, i.e. $\Delta y \approx 0$. The fitting parameters are $k_1 = 1.68$ and $k_2 = 2$. The dependence of J on Δy^2 is likely due to the fact that J depends on the square of the actual crack path, ΔS^2, such that $J \propto \Delta S^2 = \Delta a^2 + \Delta y^2$.

The results presented in Fig. 6 highlight the motivation to control microstructures in order to increase the extent of crack deflection. One way to achieve this is by introducing anisotropic grain morphology in which the weak grain boundaries are preferentially inclined at an angle with respect to the cross section of the crack growth direction. To illustrate this and to assess the contribution of grain orientation on enhancing crack growth resistance, a grain structure with an aspect ratio of 1:5 in the crack growth direction was generated.

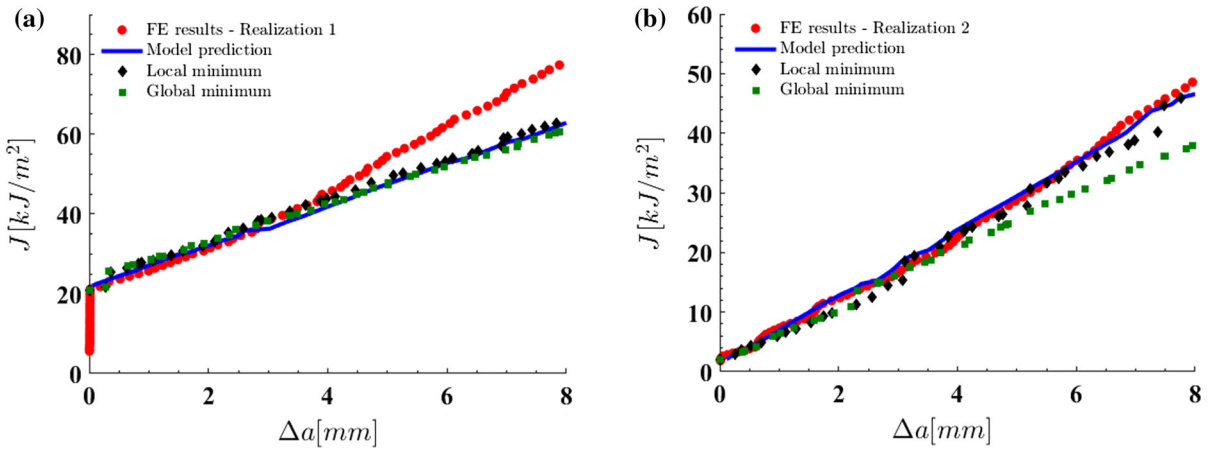

Fig. 4 Comparison of crack growth resistance curves obtained from the microstructure-based finite element calculations (FE results) and predicted using the proposed model when following the same crack path as obtained from the finite element calculations (Model prediction), when following the crack path of global minimum crack growth resistance (Global minimum) and when following the path of local minimum crack growth resistance (Local minimum) for two realizations of the specified grain microstructure: **a** realization 1 and **b** realization 2

Next, the grain microstructure was rotated such that the crack growth direction is oriented at an angle θ_g with respect to the long axis of the grains. The elongated grain morphology and the specified microstructure rotated at an angle of $\theta_g = 45°$ are shown in Fig. 7b. A comparison of the crack growth resistance curves, $J - \Delta a$, for the grain microstructures shown in Fig. 7a, obtained using the microstructure-based full field finite element calculations and the model using unit event calculations and graph search are presented in Fig. 7b. As seen in Fig. 7b the crack deflection arising as a result of highly anisotropic grain morphology has a significant toughening effect. In addition, the results also highlight the predictive capabilities of the model using unit event calculations and graph search.

In the previous example the focus was on large crack deflection away from the crack propagation direction. The crack growth resistance can also be increased by increasing the extent of crack meandering. The model proposed here only requires a series of discrete events, namely the deflection angle and grain boundary facet length. To illustrate the effect of crack meandering, we focus on the deflection angle, ψ, and assume a rather uniform grain boundary facet length. In particular, we assume that during the crack propagation process, the angle of the grain boundaries the crack encounters have a known distribution and take the distribution to be Gaussian. The Gaussian distribution is taken to be centered around $\psi_{mean} = 60°$, corresponding to an equiaxed hexagonal structure. Various values of the standard deviation are considered, $\sigma = 5°$, $15°$, $20°$ and the grain facet length is taken to be 160 μm. The deflection angle distributions were sampled and the obtained angle along with facet length is used to calculate the increment in J resulting from a propagation event. The process is repeated until achieving a specified amount of crack growth (in this case $\Delta a = 6$ mm). For each distribution, 10,000 possible trajectories were extracted and the mean, along with the 95% confidence level were calculated. The results are presented in Fig. 8. Increasing the probability of encountering large deflection angles leads to a broadening of the 95% confidence interval. In addition, the lower bound increases with increasing standard deviation σ. This implies that the larger the deviation is from an equiaxed structure, the tougher the material is. To validate the model predictions microstructure-based full field finite element calculations were carried out for a microstructure consisting of grains with a mean facet length 160 μm and an angle distribution with $\psi_{mean} = 60°$ and $\sigma = 17°$. The crack growth resistance curve obtained from the finite element calculation are compared with the model predictions in Fig. 8. The crack growth resistance curve obtained from finite element calculation falls within the confidence limits of the $\sigma = 15°$ and $\sigma = 20°$. The results presented in Fig. 8 show that the model based on

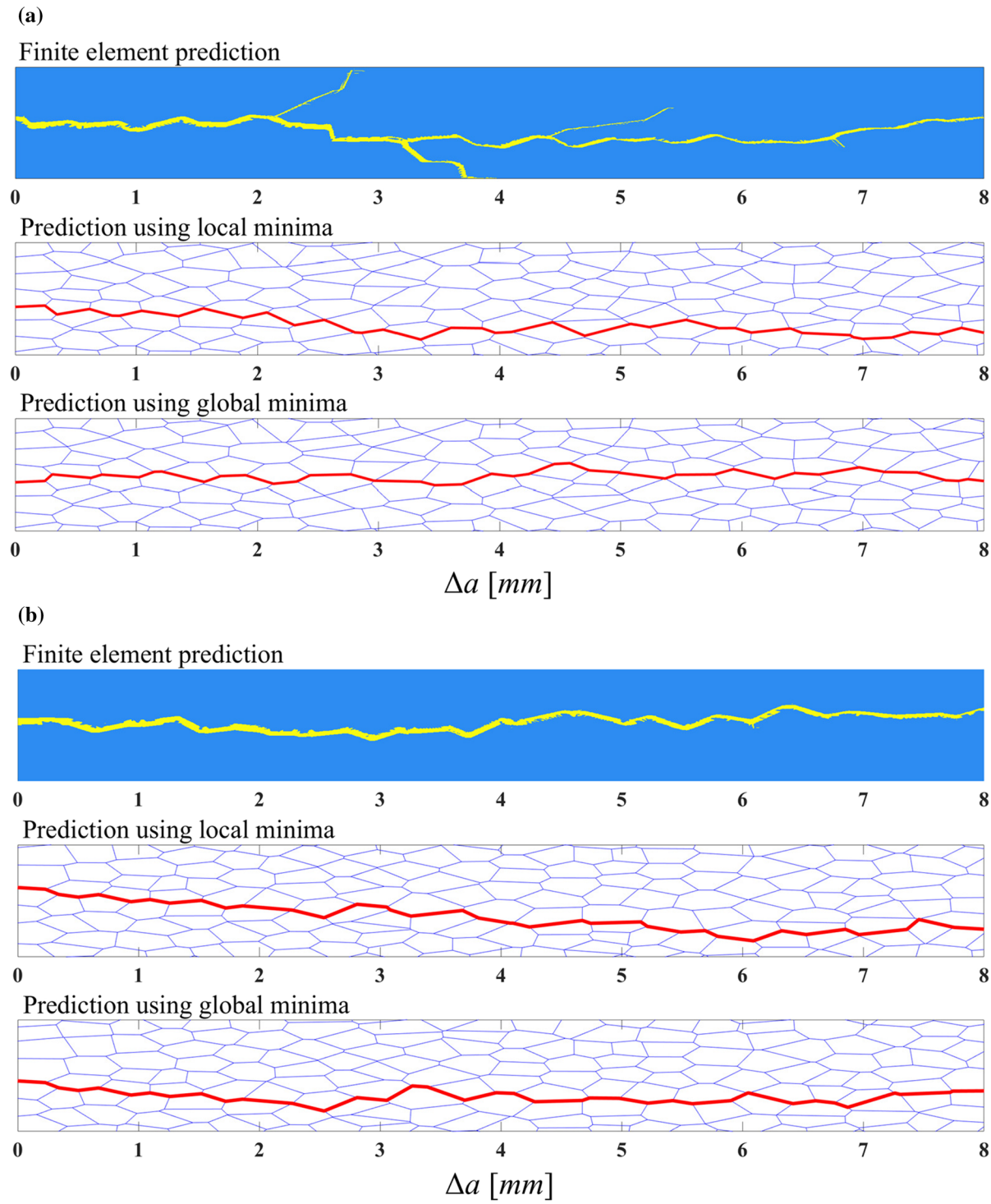

Fig. 5 Crack paths obtained from the microstructure-based finite element calculations and predicted using the proposed model based on global minimum crack growth resistance and local minimum crack growth resistance for two realizations of the specified grain microstructure: **a** realization 1 and **b** realization 2

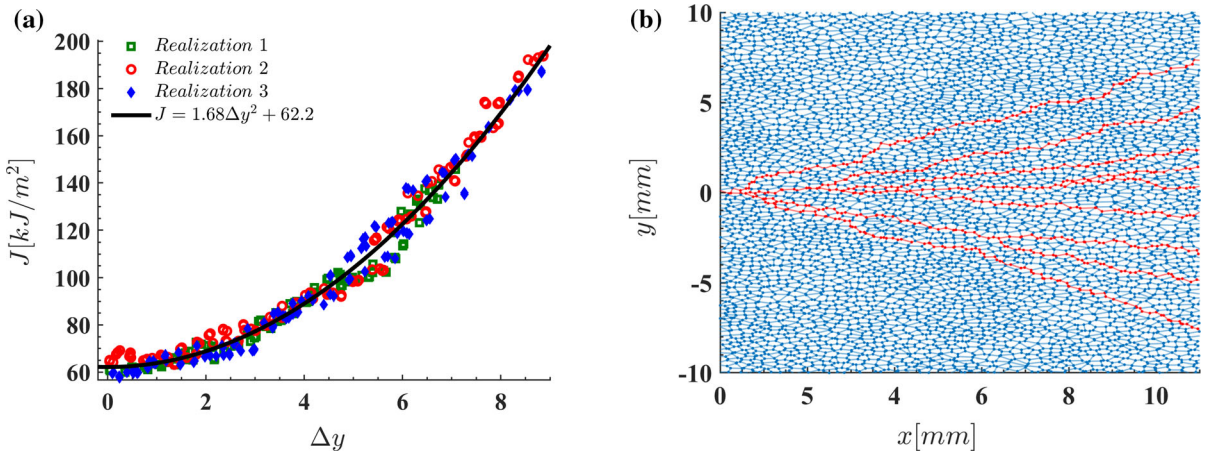

Fig. 6 **a** The dependence of overall crack growth resistance, J, for a specified amount of projected crack extension, Δa, along the crack propagation direction (x-axis) on the overall crack deflection, Δy, from the crack propagation direction for three realizations of a specified grain microstructure. **b** The crack paths corresponding to the crack growth resistance for realization 1 of the grain microstructure

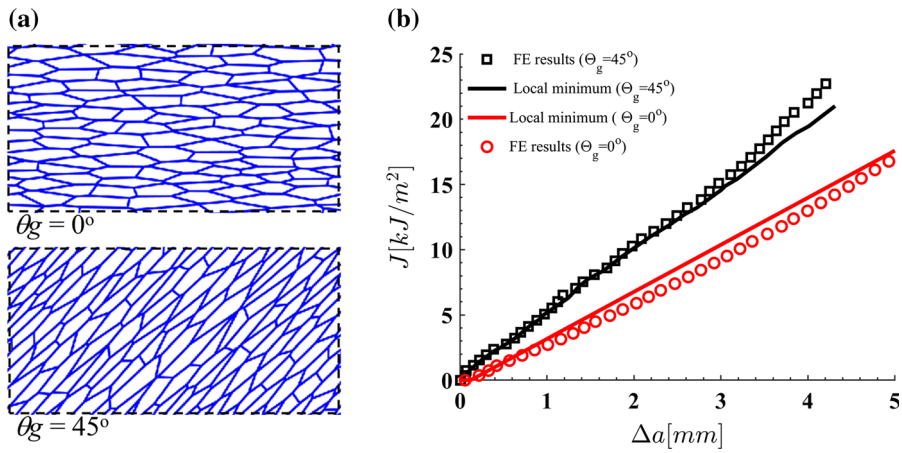

Fig. 7 **a** The elongated grain microstructure with an aspect ratio of 1:5 and rotated at an angle of $\theta_g = 0°$ and 45° with respect to the crack growth direction. **b** Comparison of the crack growth resistance curves obtained using the microstructure-based finite element calculations and predicted using the proposed model when following the path of local minimum crack growth resistance for the two microstructures

unit events and graph search can also be used to assess the overall crack growth resistance of the materials with a known distribution of grain morphology.

6 Concluding remarks

With the emergence of advanced manufacturing technologies such as additive manufacturing (Herderick 2011; Frazier 2014) or others (Hosokawa et al. 2013) it is becoming increasingly possible to control the microstructural features of metallic alloys. In addition, the emergence of 3D tomography techniques (Uchic et al. 2007; Ueda et al. 2014; Kahziz et al. 2016) make it possible to characterize the microstructural features of a material in great detail. The capability to characterize and control microstructural features provides a motivation for developing methodologies for designing material microstructures with improved properties. In this work, for materials that are prone to grain boundary ductile fracture, we have developed a methodology for designing grain microstructures with improved crack growth resistance. The proposed model is based on discrete unit events and graph search. The discrete unit event associated with grain boundary fracture is the propagation of a crack from one grain boundary junction to the another. The "cost" in terms of the change in J, associated with each unit event is used to construct a graph in both Euclidean and J-resistance space. The

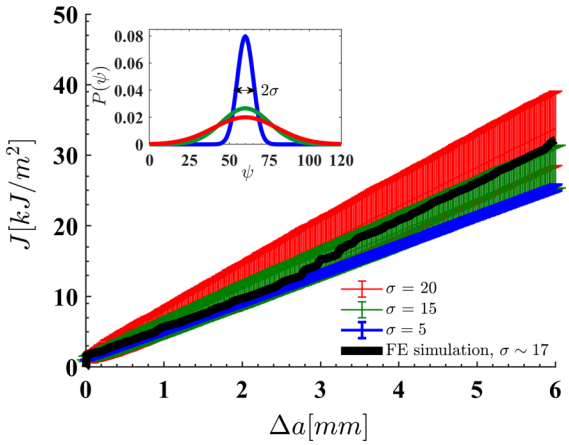

Fig. 8 The 95% confidence envelope for the crack growth resistance curves of a grain boundary network with a facet length of $da = 160\,\mu m$ and a Gaussian distribution of deflection angles with a mean of $\Psi = 60$ and a standard deviation of: $\sigma = 5$ (blue); $\sigma = 15$ (green); $\sigma = 20$ (red). The results of a FE simulation for a grain microstructure with the same average facet length and $\sigma = 17$ is shown for comparison (black)

directed graph in J-resistance space contains information on the crack growth resistance curve of all possible crack paths in the microstructure. The crack path for a specified amount of crack growth is then estimated as the crack path dictated by either global minimum or local minimum crack growth resistance criteria. The predictive capability of the proposed model is validated against results of full field microstructure-based finite element calculations. The comparison of the results obtained from the finite element calculations and those predicted using the proposed model highlights the fact that the crack path is largely dictated by the local minimum crack growth resistance at each grain boundary junction and not by the global minimum crack growth resistance.

In a broad range of areas of microstructural design, grain boundaries have attracted considerable attention. Grain boundaries are an extremely important heterogeneity in many structural alloys and metals that can be controlled (in a statistical manner) both in terms of spatial arrangement and grain boundary character. The ability of polycrystalline materials to resist failure under extreme environmental and mechanical loads is strongly correlated with the grain boundaries network they poses (Kim et al. 2003; Kobayashi et al. 2014; Takahashi et al. 2016). Stress corrosion cracking, hydrogen embrittlement and low damage tolerance are all dominated by the grain boundaries (Kim et al. 2006; Kobayashi et al. 2012; Arafin and Szpunar 2009).

Over the past decades, our understanding of the relation between specific grain boundaries and their resistance to the aforementioned processes has increased along with the ability to choose processing routes leading to specific grain boundary character distributions, geometrical properties of the grains and chemical parameters (Randle and Owen 2006; Cantwell et al. 2016). However, designing an optimum grain boundary network to improve material properties involves optimizing the topological features of the material microstructure. The (limited) available computational techniques are extremely time consuming so that direct coupling of such calculations with an iterative optimization scheme is not practical. We hope that our computationally inexpensive model can be used in an iterative, non-gradient topological optimization scheme to design material microstructures with improved intergranular fracture resistance. Additionally, the model can be used to predict the path and resistance of any crack growth process that discretely propagates from one grain boundary junction to another, or to predict the overall crack growth resistance of materials with a known distribution of grain boundary orientations and grain boundary lengths.

Acknowledgements The financial support provided by the Pazy foundation young researchers award Grant # 1176 (SO), U.S. National Science Foundation Grant CMMI - 1663130 (AS), and European Union's Horizon2020 Programme (Excellent Science, Marie-Sklodowska - Curie Actions, H2020 - MSCA - RISE - 2017) under REA Grant agreement 777896 (Project QUANTIFY, SO and AS) are gratefully acknowledged. We are also grateful for the high performance research computing resources provided by Texas A&M University.

References

Arafin MA, Szpunar JA (2009) A new understanding of intergranular stress corrosion cracking resistance of pipeline steel through grain boundary character and crystallographic texture studies. Corros Sci 51:119–128

Belytschko T, Chiapetta RL, Bartel HD (1976) Efficient large scale non-linear transient analysis by finite elements. Int J Numer Methods Eng 10:579–596

Bendsøe MP, Kikuchi N (1988) Generating optimal topologies in structural design using a homogenization method. Comput Methods Appl Mech Eng 71:197–224

Bendsøe MP, Sigmund O (2004) Topology optimization: theory, methods, and applications, 2nd edn. Springer, Berlin

Cantwell PR, Ma S, Bojarski SA, Rohrer GS, Harmer MP (2016) Expanding time temperature-transformation (TTT)

diagrams to interfaces: a new approach for grain boundary engineering. Acta Mater 106:78–86
Chapman CD, Saitou K, Jakiela MJ (1994) Genetic algorithms as an approach to configuration and topology design. J Mech Des 116:1005–1012
Cheng G, Jiang Z (1992) Study on topology optimization with stress constraints. Eng Optim 20:129–148
Dijkstra EW (1959) A note on two problems in connexion with graphs. Numerische Mathematik 1:269–271
Frazier WE (2014) Metal additive manufacturing: a review. J Mater Eng Perform 23:1917–1928
Fullwood DT, Niezgoda SR, Adams BL, Kalidindi SR (2010) Microstructure sensitive design for performance optimization. Prog Mater Sci 55:477–562
Gurson AL (1975) Plastic flow and fracture behavior of ductile materials incorporating void nucleation, growth and interaction. Ph.D. thesis, Brown University, Providence, RI
Hao S, Moran B, Liu WK, Olson GB (2003) A hierarchical multi-physics model for design of high toughness steels. J Comput Aided Mater Des 10:99–142
Hao S, Liu WK, Moran B, Vernerey F, Olson GB (2004) Multi-scale constitutive model and computational framework for the design of ultra-high strength, high toughness steels. Comput Methods Appl Mech Eng 193:1865–908
Herderick E (2011) Additive manufacturing of metals: a review. In: Proceedings of MS&T'11. Additive Manufacturing of Metals, Columbus, OH
Hosokawa A, Wilkinson DS, Kang J, Maire E (2013) Onset of void coalescence in uniaxial tension studied by continuous X-ray tomography. Acta Mater 61:1021–1036
Hyun S, Torquato S (2001) Designing composite microstructures with targeted properties. J Mater Res 16:280–285
James KA, Waisman H (2014) Failure mitigation in optimal topology design using a coupled nonlinear continuum damage model. Comput Methods Appl Mech Eng 268:614–631
Kahziz M, Morgeneyer TF, Mazire M, Helfen L, Bouaziz O, Maire E (2016) In situ 3D synchrotron laminography assessment of edge fracture in dual-phase steels: quantitative and numerical analysis. Exp Mech 56:177–195
Kim T, Hong KT, Lee KS (2003) The relationship between the fracture toughness and grain boundary character distribution in polycrystalline NiAl. Intermetallics 11:33–39
Kim CS, Rollett AD, Rohrer GS (2006) Grain boundary planes: new dimensions in the grain boundary character distribution. Scr Mater 54:1005–1009
Kirsch U (1990) On singular topologies in optimum structural design. Struct Optim 2:133–142
Kobayashi S, Maruyama T, Tsurekawa S, Watanabe T (2012) Grain boundary engineering based on fractal analysis for control of segregation-induced intergranular brittle fracture in polycrystalline nickel. Acta Mater 60:6200–6212
Kobayashi S, Maruyama T, Saito S, Tsurekawa S, Watanabe T (2014) In situ observations of crack propagation and role of grain boundary microstructure in nickel embrittled by sulfur. J Mater Sci 49:4007–4017
Kulkarni AJ, Krishnamurthy K, Deshmukh S, Mishra R (2004) Microstructural optimization of alloys using a genetic algorithm. Mater Sci Eng A 372:213–20
Larsen UD, Signund O, Bouwsta S (1997) Design and fabrication of compliant micromechanisms and structures with negative Poisson's ratio. J Microelectromech Syst 6:99–106
Lee CY (1961) An algorithm for path connections and its applications. IRE Trans Electron Comput 3:346–365
Liu R, Kumar A, Chen Z, Agrawal A, Sundararaghavan V, Choudhary A (2015) A predictive machine learning approach for microstructure optimization and materials design. Sci Rep 5:11551
Lütjering G, Williams JC (2007) Titanium, 2nd edn. Springer, Berlin
Mantri SA, Choudhuri D, Behera A, Cotton JD, Kumar N, Banerjee R (2015) Influence of fine-scale alpha precipitation on the mechanical properties of the beta titanium alloy beta-21S. Metall Mater Trans A 46:2803–2808
McDowell DL (2007) Simulation-assisted materials design for the concurrent design of materials and products. JOM 59:21–5
McDowell DL, Olson GB (2009) Concurrent design of hierarchical materials and structures. Scientific modeling and simulations. Springer, Dordrecht, pp 207–40
Needleman A, Tvergaard V, Bouchaud E (2012) Prediction of ductile fracture surface roughness scaling. J Appl Mech 79:031015
Olson GB (1997) Computational design of hierarchically structured materials. Science 277:1237–42
Osovski S, Srivastava A, Williams JC, Needleman A (2015a) Grain boundary crack growth in metastable titanium β alloys. Acta Mater 82:167–178
Osovski S, Srivastava A, Ponson L, Bouchaud E, Tvergaard V, Ravi-Chandar K, Needleman A (2015b) The effect of loading rate on ductile fracture toughness and fracture surface roughness. J Mech Phys Solids 76:20–46
Pan J, Saje M, Needleman A (1983) Localization of deformation in rate sensitive porous plastic solids. Int J Fract 21:261–278
Paris PC, Tada H, Zahoor A, Ernst H (1979) The theory of instability of the tearing modes in elastic-plastic crack growth. In: Landes JD, Begley JA, Clarke GA (eds) Elastic-plastic fracture, ASTM STP 668. American Society for Testing and Materials, pp 5–36
Peirce D, Shih CF, Needleman A (1984) A tangent modulus method for rate dependent solids. Comput Struct 18:875–887
Randle V, Owen G (2006) Mechanisms of grain boundary engineering. Acta Mater 54:1777–1783
Rice J (1968) A path-independant integral and the approximate analysis of strain concentration by notches and cracks. J Appl Mech 35:379–386
Sigmund O, Torquato S (1997) Design of materials with extreme thermal expansion using a three-phase topology optimization method. In: Smart structures and materials' 97. International Society for Optics and Photonics, pp 52–60
Sigmund O, Torquato S, Aksay IA (1998) On the design of 1-3 piezocomposites using topology optimization. J Mater Res 13:1038–1048
Srivastava A, Ponson L, Osovski S, Bouchaud E, Tvergaard V, Needleman A (2014) Effect of inclusion density on ductile fracture toughness and roughness. J Mech Phys Solids 63:62–79
Srivastava A, Osovski S, Needleman A (2017) Engineering the crack path by controlling the microstructure. J Mech Phys Solids 100:1–20
Takahashi Y, Kondo H, Asano R, Arai S, Higuchi K, Yamamoto Y, Muto S, Tanaka N (2016) Direct evaluation of grain

boundary hydrogen embrittlement: a micro-mechanical approach. Mater Sci Eng A 661:211–216
Torquato S (2005) Microstructure optimization. Handbook of materials modeling. Springer, Berlin, pp 2379–2396
Torquato S, Hyun S (2001) Effective-medium approximation for composite media: realizable single-scale dispersions. J Appl Phys 89:1725–1729
Tvergaard V (1981) Influence of voids on shear band instabilities under plane strain conditions. Int J Fract 17:389–407
Tvergaard V (1982a) On localization in ductile materials containing spherical voids. Int J Fract 18:237–252
Tvergaard V (1982b) Influence of void nucleation on ductile shear fracture at a free surface. J Mech Phys Solids 30:399–425
Tvergaard V, Needleman A (1984) Analysis of the cup-cone fracture in a round tensile bar. Acta Metall 32:157–169
Uchic MD, Holzer L, Inkson BJ, Principe EL, Munroe P (2007) Three-dimensional microstructural characterization using focused ion beam tomography. MRS Bull 32:408–416
Ueda T, Helfen L, Morgeneyer T (2014) In situ laminography study of three-dimensional individual void shape evolution at crack initiation and comparison with Gurson–Tvergaard–Needleman-type simulations. Acta Mater 78:254–270
van Dijk NP, Maute K, Langelaar M, Van Keulen F (2013) Level-set methods for structural topology optimization: a review. Struct Multidiscip Optim 48:437–472
Williams JC, Froes FH, Chesnutt JC, Rhodes CG, Berryman RG (1978) Development of high fracture toughness titanium alloys. Toughness and fracture behavior of titanium, ASTM STP 651. American Society for Testing and Materials, pp 64–114
Xia L, Breitkopf P (2015) Design of materials using topology optimization and energy-based homogenization approach in Matlab. Struct Multidiscip Optim 52:1229–1241